Science of the Total Environment 741 (2020) 140411

Contents lists available at ScienceDirect

Science of the Total Environment

journal homepage: www.elsevier.com/locate/scitotenv

The biosorption of mercury by permeable pavement biofilms in stormwater attenuation

Alireza Fathollahi [a,*], Stephen J. Coupe [a], Amjad H. El-Sheikh [b], Luis A. Sañudo-Fontaneda [a,c]

[a] Centre for Agroecology Water and Resilience (CAWR), Coventry University, Wolston Lane, Ryton on Dunsmore, CV8 3LG, UK
[b] Department of Chemistry, Faculty of Science, The Hashemite University, Al-Zarqa 13115, Jordan
[c] Department of Construction and Manufacturing Engineering, Institute of Natural Resources and Territorial Planning, University of Oviedo, Campus of Mieres, Calle Gonzalo Gutiérrez Quirós s/n,33600 Mieres (Asturias), Spain

HIGHLIGHTS

- We tested whether living biofilm layer would remove Hg(II) in urban runoff.
- The biofilm provided different biosorp tion capacities during development stages.
- Hg removal by biofilm was spontaneous, exothermic, and thermodynamically feasible.
- Living biofilm removed Hg(II) with a physical biosorption mechanism.
- Amine, hydroxyl, and carboxyl groups were Hg biosorption agents of living biofilm.

GRAPHICAL ABSTRACT

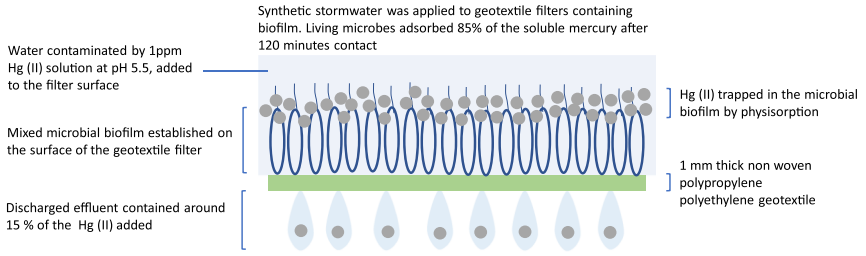

ARTICLE INFO

Article history:
Received 4 May 2020
Received in revised form 19 June 2020
Accepted 19 June 2020
Available online 20 June 2020

Editor: Mae Sexauer Gustin

Keywords:
Hg(II)
Biofilm
Biosorption
Kinetics
Geotextile
SuDS

ABSTRACT

This study reports on the evaluation of the equilibrium, thermodynamics and kinetics of mercury (II) biosorption using a living biofilm, developed on a nonwoven polypropylene and polyethylene geotextile, typically used within the structure of Sustainable Drainage System (SuDS) devices. Batch biosorption assays were carried out with variables such as pH, initial concentrations, contact time, temperature and biofilm incubation time. Langmuir, Freundlich and Dubinin Radushkevich (D-R) models were applied to the equilibrium data which revealed the maximum biosorption capacities and efficiencies at pH 5.5 with a contact time of 120 min at 25 °C. With 20 mg L^{-1} added Hg (II), living biofilm samples with incubation times of 1, 7, 14, 21 and 28 days, biosorption values were 101.31 (55.72%), 24.41 (67.12%), 16.81 (61.37%), 9.70 (62.57%) and 13.34 (65.38%) mg g^{-1}, respectively. Free mean biosorption energy from the D-R model was between 2.24 and 2.36 kJ mol^{-1} for all biofilm development incubation times, that revealed the physical biosorption mechanism for Hg(II). The thermodynamic studies showed that the Hg(II) biosorption of living biofilm was thermodynamically feasible and had a spontaneous and exothermic nature. Kinetic parameters revealed that Hg(II) biosorption onto living biofilm had a good correlation with a pseudo second-order kinetic model. FTIR spectra after biosorption suggested that amine, hydroxyl and carboxyl groups were the main functional groups available and responsible for Hg(II) biosorption onto living biofilm. Experimental data suggested that a living biofilm developed on a nonwoven polypropylene and polyethylene geotextile can be efficient in the removal of mercury ions from contaminated urban and industrial runoff.

* Corresponding author.
E-mail address: ad2068@coventry.ac.uk (A. Fathollahi).

https://doi.org/10.1016/j.scitotenv.2020.140411

1. Introduction

Sustainable Drainage Systems (SuDS) are designed to manage runoff volume as well as to reduce urban water pollution (Ashley et al., 2015; Woods Ballard et al., 2015). Improving water quality is defined as the pollutant removal efficiency by detention of suspended solids, nutrients and trapping of particulate phase metals (Allen et al., 2017).

Newman et al. (2002) reported that SuDS such as permeable pavement systems (PPS) are efficient in-situ aerobic bio-reactors, as demonstrated by their retention and biodegradation of lubricating mineral oil. This has been confirmed by respirometry, oil in effluent results, and microbiological investigations showing high microbial numbers and biodiversity, and scanning electron microscopy showing well developed biofilms. Newman et al. identified a significant knowledge gap in the field of stormwater management and the investigation of the main physical and biological processes occurring within the system and how they contributed to water quality performance. The work by Coupe et al. (2003) increased the knowledge on microbiological functions in PPS and the impact of microbes on hydrocarbon biodegradation, PPS biofilms reaching removal efficiencies up to 98.7%, with all microbial groups in the PPS contributing to the oil removal. This research opened a new perspective for SuDS, where geotextiles were shown to play a central role, including the work of Spicer et al. (2006) that explored potential uses of this layer as a medium for slow-release phosphate beads that have been shown to maintain nutrient balance and to maintain bacterial communities that biodegrade the oil in PPS. Gomez-Ullate et al. (2010) highlighted the impact of different types of geotextile on the water management properties of car parks using PPS. Other developments (Nnadi et al., 2014) demonstrated that geotextiles improved infiltration and volume attenuation, which contributed to an increase in the treatment time; also improving the quality of stormwater that could be stored and later used for irrigation.

Mbanaso et al. (2013) and Theophilus et al. (2018) investigated the impact of glyphosate based herbicides and fertilisers on the removal efficiency capacity of the geotextile layer and Mbanaso et al. (2020) demonstrated that the concentration of metals in the different layers of a PPS containing a geotextile, found in the structure by the end of the operational life, were below the regulatory limits indicated by the FAO for irrigation purposes. This finding suggested that PPS aggregates might be reused, not disposed of after single use due to the perceived environmental risk presented by the presence of remaining metals and organics.

Metal concentrations in urban runoff have been widely studied for roads and trafficked areas, to identify the main causes of their occurrence and the impact they have on receiving systems. Heavy metals can occur in the dissolved phase and this represents a knowledge gap, regarding the way stormwater management systems remove dissolved metals (Huber et al., 2016). Vadas et al. (2017), tested a method for improving the dissolved metal trapping abilities of pervious concrete, by adding sorbents to the concrete mixture, and reported removal efficiencies of 85–95%, 30–95%, 60–90% and 95+% for dissolved Cu, Zn, Cd and Pb respectively in synthetic stormwater.

Water pollution derived from industrialisation and urbanisation has increased significantly in the past decade (Rajeshkumar et al., 2018). Rodriguez Martin et al. (2015) reported a substantial increase of metal concentrations in urban areas due to human activities with Cd, Ni and Cr concentrations 10, 13 and 16 times higher than in 1941. Mercury (Hg) is generally considered to be one of the most toxic heavy metals, eventually discharged into stormwater as a result of human activities, and is a threat to humans and the environment (Nascimento and Chartone-Souza, 2003).

Several studies have addressed the presence of mercury concentrations in storm water and street dust. Lawson et al. (2001) reported higher concentrations of mercury in rivers passing through cities (22 $\mu g\ m^{-2}\ yr^{-1}$) than in rural rivers (1.35 $\mu g\ m^{-2}\ yr^{-1}$). In a research on the concentration of mercury in street dust of Nanning, China, moderate to heavy pollution ($338 \pm 222\ \mu g\ kg^{-1}$) has been reported (Lin et al., 2019). In recent decades, contaminated runoff has been an area of interest due to its importance and influence on water quality in urban and rural catchments, encouraging researchers to look for toxic compounds in urban runoff (Gill et al., 2014; Han et al., 2014; Borne et al., 2014). According to a USEPA report (EPA-452/R-97-005) this phenomenon is a result of two main factors. First, various sources release mercury into the environment and a huge increase of impermeable surface area in cities, generates contaminated runoff which is conveyed to surface and underground water receptors.

In general, several methods are used for heavy metal removal from effluent, including chemical precipitation, oxidation or reduction, filtration, ion exchange, electrochemical approaches and membranes, that are either ineffective or expensive (Green-Ruiz et al., 2008; Tsekova et al., 2010). In contrast with the above methods, biosorption is considered as a cost effective and low energy pollution treatment method that involves microbial communities in the process of runoff decontamination. Bacteria, fungi, algae, and activated sludge have been under investigation as potential biosorption agents for the removal of mercury available in aqueous systems in recent years (Rani et al., 2010; Subhashini et al., 2011; Viraraghavan and Srinivasan, 2011; Mamisahebei et al., 2007). The biosorption efficiency of biomass is reliant on prevailing environmental conditions such as temperature, pH, and contact time (Volesky, 2003).

It is well understood that different chemical compounds can alter biofilm structure and function (Sabater et al., 2007). The effects of heavy metals on biofilm structures include shift in taxonomic groups, morphological conversions, and also changes in biomass growth (Sabater et al., 2007). Biofilm exposure to Hg differentially distresses taxonomic groups and leads to the growth of a biofilm with more mercury tolerance (Blanck and Dahl, 1996). Peres et al. (1997) observed a 2.5-fold reduction of cell size in microorganisms exposed to 1.5–2 $\mu g\ L^{-1}$ Hg. However, Extracellular Polymeric Substance (EPS) acts as a shield in biofilm and protects the bacteria (Najera et al., 2005). Studies have shown that exposure to Hg ions will disturb microbial metabolism (Le Faucheur et al., 2014). The metabolic blockage can lead to faster breakdown of the biofilm and as a result, the biofilm will more readily slough off the surface (Scott et al., 1995). However, there is a lack of sufficient experimental research addressing to what extent and at what concentration, biofilm sloughs off in interaction with heavy metals.

In order to achieve sustainability within road construction, it is best practice design to approach a contaminated runoff remediation method within or adjacent to, the structure of the pavement. Geotextiles are widely used in porous pavements as a barrier to contain fine aggregates travelling through the pavement structure and to promote water infiltration.

The use of geotextiles in SuDS has been mainly focused on highway filter drains (HFD) and PPS (Abbar et al., 2017; Sañudo Fontaneda et al., 2016). The distance from the surface of the pavement of the geotextile is important in the performance both of volume attenuation (Sañudo-Fontaneda et al., 2018) and water quality (Zhao et al., 2018). However, more research is necessary to find out to what extent dissolved metals are influenced by interaction with a geotextile, and whether or not the presence of a biofilm on the geotextile makes a difference to the rate and extent of metal removal.

In this study, the feasibility of growing a living, mixed species biofilm on the structure of a nonwoven polypropylene and polyethylene geotextile, widely used in sustainable drainage systems was investigated. After establishing a biofilm on the geotextile, the main aim of the research was to measure the efficiency of this layer in the biosorption of emerging heavy metals, present in urban runoff, in this case mercury. Mercury was chosen as the analyte of interest in this work for two main reasons. Firstly, it is a non-biologically useful metal which is toxic in some degree to all living things, and secondly, it does not form a part of microbial biomass unless it is contributed by exogenous sources, typically from contaminated water. Mercury is also a substance of interest in

SuDS due to its toxicity and the high probability of it occurring in stormwater as discussed by Lodeiro et al. (2019).

We listed three main questions from the scope of this study:

1. What are the biosorption efficiencies of different stages of living biofilm growth?
2. What are the factors controlling the biosorption of Hg(II) by the living biofilm?
3. What physical and chemical processes are taking place during the biosorption and what are the kinetics and thermodynamic of the Hg(II) biosorption?

Question 1 and 2 are evaluated by conduction batch biosorption experiments in different physical and environmental conditions. Question 3 is addressed by analyzing the data from different experimental assays using thermodynamic, kinetics and various analytical techniques.

2. Materials and methods

2.1. Chemicals and reagents

Different concentrations of mercury solutions were prepared by adding appropriate volumes of a 1000 mg L^{-1} stock Hg (II) in 2% HNO_3 solution into deionised water, prior to pH adjustment where necessary. The analytical grade Hg(II) stock solution used in this research was provided by Perkin Elmer (Waltham, Massachusetts, United States). Analytical grade sodium hydroxide (Sigma Aldrich, 98% purity) was used to prepare 0.5 M NaOH solution for the purpose of pH adjustment. Analytical grade 70% nitric acid solution was used to prepare samples prior to analysis (Fisher Scientific, Waltham, Massachusetts, United States).

2.2. Biofilm reactor system

2.2.1. Preparation of geotextile sheets and biofilm reactor

In this research a conventional geotextile layer used in Sustainable Drainage Systems (SuDS) was used as the biofilm substratum. Properties of the employed non-woven geotextile with a composition of 70% polypropylene and 30% polyethylene are presented in Table Supporting Information (SI) 1.

Geotextile sheets were cut into circles with a surface area of 65 cm^2 prior to biofilm bioreactor setup. All geotextile circles were washed, labelled and the weights were measured using a 5 decimal place scale (Sartorius analytical scale), prior to their addition to the bioreactor. The lab scale experimental bioreactor was a 12-litre plastic container equipped with two air pumps fixed in the base to provide aerobic condition for the microbial growth. This installation provided the required oxygen for microorganisms and caused the circulation of oxygen and microbial culture.

2.2.2. Composition of the growth medium

The laboratory scale reactor in this research operated using 10 L of medium with the following composition: 9800 mL of deionised water, 200 mL of mixed microbial culture liquid containing microorganisms isolated from an established pervious pavement system in Coventry (UK) including oil degrading microbes, 10 g engine oil and 28 mL liquid plant food containing 14% Nitrogen (N) and 3% phosphorus (P) as resources for bacterial growth. This medium composition was used for all assays carried out in this study.

2.2.3. Operating conditions

In order to keep aerobic conditions within the reactor medium during biofilm growth, the liquid in the reactor was aerated on regular basis to keep dissolved oxygen (DO) in range of 4–6 mg L^{-1}. The bioreactor medium pH was kept in the range of 7–8 at 20 °C away from light to prevent the growth of algae. Geotextile sheets were harvested after varying incubation times (1, 7, 14, 21, and 28 days).

2.3. Equilibrium biosorption experiments

In this research, the biosorption capacity of different concentrations of Hg (II) (1, 2, 5, 10, 20 mg L^{-1}) by a living biofilm grown on a non-woven polypropylene and polyethylene geotextile was studied with different pH values (2, 3, 4, 5, 6, 7) and incubation times (1, 7, 14, 21 and 28 days growth in a bioreactor). Biosorption experiments were carried out after harvesting the geotextile circles from the biomass reactor. 10 mL of different concentrations of Hg (II) in deionised water were applied to harvested geotextile circles where the pH of the mixture was adjusted using 0.5 M NaOH and filtered through the permeable geotextile after 120 min of contact time. All adsorption experiments were carried out with 20 replicates alongside control and blank samples at a controlled of 25 °C. Samples were collected and the Hg concentration was measured by use of a Perkin-Elmer optima 5300 DV ICP-OES. Hg (II) concentrations in samples were measured in triplicate at three wavelengths. After taking the samples, the geotextile circles were oven dried at 60 °C prior to weight measurement and biofilm mass calculations. Due to the nature of the biofilm growth on geotextiles and uncertainty about the mass of biofilm on geotextiles, all assays were done with 20 replicates in order to calculate a representative average biofilm mass and adsorption rate.

2.4. Modelling of biosorption experiments

Langmuir (1916) and Freundlich (1906) isotherm equations were used to model the biosorption data. The Langmuir equation (in its linear form) is given by the equation:

$$C_e/q_e = (1/q_{max}) \cdot C_e + 1/(q_{max} \cdot K_L)$$

where q_e is the surface Hg(II) concentration on the biofilm (mg g^{-1}), C_e is the concentration of Hg (II) at equilibrium in the solution (mg L^{-1}), q_{max} is the maximum biosorption capacity of the biofilm (mg g^{-1}), K_L is the affinity of Hg (II) binding on biofilm (L mg^{-1}) (Sweileh et al., 2014).

The Freundlich isotherm is given by the linear equation:

$$\log q_e = (1/n) \cdot \log C_e + \log K_F$$

where K_F and n are biosorption extension and nonlinearity indicators which are evaluated by plotting log q_e vs. log C_e and calculating slope and intercept (El-Sheikh et al., 2012).

q_e was calculated using the following equation:

$$q_e = (C_0 - C_e)\left(\frac{V}{M}\right)$$

where V is the volume of Hg (II) solution applied to biofilm (L), C_o is the initial concentration of Hg(II) (mg L^{-1}), C_e is the concentration of Hg (II) in solution at equilibrium (mg L^{-1}) and M is the dry weight of the biosorbent (g). The dry weight of biofilm in this study was measured by weighing the dry and clean geotextile circles before and after biofilm development. All labelled geotextile circles were collected after the biosorption experiment and were placed in 60 °C oven for 72 h to obtain the dry weight of biofilm to be used in data evolution.

2.5. Effect of temperature on biosorption (thermodynamic studies)

Thermodynamic analysis and effect of temperature on Hg (II) biosorption was carried out at 25, 35, 45 and 55 °C, pH 5.5 and 120 min contact time with the same experimental set-up described in Section 2.3. After the measurement of Hg (II) concentrations at equilibrium, thermodynamic parameters were calculated.

2.6. Control biosorption experiment

At all stages of biosorption experiments including the effect of pH, incubation time, and initial Hg (II) concentration on biosorption capacity, 20 geotextile circles with the same physical conditions were soaked in synthetic media of deionised water and the same concentration of oil which was used in the bioreactor. The same procedure described in Section 2.3 was applied after harvesting the geotextiles at the same time interval as the biofilm carrying geotextiles. Samples were preserved for ICP-OES analysis. These control experiments were carried out to evaluate possible interaction of geotextile and oil in deionised water without any microorganisms (no biofilm) and compare the Hg (II) sorption capacities of geotextiles with and without biofilm.

2.7. Kinetic biosorption experiments

Biosorption kinetic studies were carried out to evaluate the minimum contact time required to reach equilibrium in metal biosorption and calculate the rate of Hg(II) ions bonding to the biofilm. Results from the kinetics reveal the complex mechanism of biosorption. Mercury biosorption by living biomass was carried out at various contact times (0, 5, 10, 15, 30, 45, 60, 75, 90, 105 and 120 min) for six different concentrations (0.2, 1.0, 2.0, 5.0, 10.0 and 20.0 mg L^{-1}) of Hg(II). All kinetic studies were conducted at pH 5.5 and 25 °C before analysis by ICP-OES. Kinetic adsorption coefficients were calculated for pseudo first-order and pseudo-second order kinetic models as described later, in the Results and discussion section. An intra-particle diffusion model was also applied as described later.

2.8. FTIR analysis

Fourier Transform Infrared (FTIR) spectroscopy was used to characterise the functional groups available on biofilm, on microbial cells, their exudates and their role in the biosorption process of Hg(II) ions. Reflection FTIR with a cooled detector technique was used in this study. Clean, biofilm grown and 20.0 mg L^{-1} Hg (II) loaded geotextile circles were analyzed using a Nicolet iN10 Infrared Microscope (Thermo Fisher Scientific) in reflection mode to analyze the absorption spectra of the bond in the range of 400 to 4000 cm^{-1}. Spectra from Hg (II) loaded and unloaded biofilm-geotextiles, were compared to identify possible functional groups available on the biofilm and occupied by Hg(II) ions.

3. Results and discussion

3.1. FTIR analysis of biofilm

FTIR analysis was carried out to evaluate the functional groups available on biofilm and compare the spectra after loading Hg(II) ions to reveal the functional groups involved in biosorption. The absorbance spectra for living biofilm and Hg(II) loaded biofilm are shown in Fig. 1, that shows shifts and peaks changes after the biosorption process. Amine groups appeared at 3200 to 3300 cm^{-1}, C═C-H links of alkene groups were observed at 3020 to 3100 cm^{-1}. The bands located at 2850 to 2975 cm^{-1} were attributed to C—H alkane groups, while the band at 1739 cm^{-1} was assigned to COO^{-} anions. Moreover, alkene C═C chains have a band within the range of 1640 to 1680 cm^{-1}. Bands located at 1550 and 1460 cm^{-1} were attributed to the N—O stretching and C—H bending groups, respectively.

Wavenumbers between 1380 and 1385 cm^{-1} were an indication of C—H links of alkane groups. Bands between 1310 and 1370 cm^{-1} were a sign of O—H bending groups and the chains at 1237 cm^{-1} were an indication of S═O antisymmetric stretching. The wavenumber 1162 cm^{-1} and bands between 1030 and 1070 cm^{-1} were assigned to C—O and S═O stretching groups, respectively. Finally, absorption bands characterizing C═C link of alkene groups appeared at wavelength 960 to 980 cm^{-1}. By comparing the spectra of biofilm before and after the Hg (II) biosorption, the following interpretations were made:

The shifting and broadening of the band associated with amine groups occurred within the range of 3280 to 3290 cm^{-1}, that characterises the presence of amine groups and interaction between Hg and N—H links on biofilm. The bands between 3300 and 3600 cm^{-1} that are associated with OH- groups, were broader after the biosorption process which is a sign of Hg complexation by biofilm. The band at 1739 cm^{-1} was attributed to loading of Hg (II) as a result of interaction with carboxylate groups. The shifting and broadening of the bands located at 1650 to 1660 cm^{-1} that represent the presence of C═C groups, indicates an interaction between Hg and C═C bonds of alkene chains. The bands located at 1385 cm^{-1} had shifted after the biosorption that is a result of interaction between alkene groups and Hg through C—H bonds. The bands located between 1150 and 1300 cm^{-1}, show that the interaction has taken place after the biosorption on alkyl halide groups as the bands shifted, stretched, and became broader after Hg and C-X bond interactions. The shifting of the bands between 1235 and 1335 cm^{-1} after the biosorption, assigned to aromatic amines, provided information on the interaction between Hg and C—N bonds available on the biofilm. The shifting, broadening, and stretching of the band at 1050–1100 cm^{-1} after the biosorption were associated with C—O bonds, the process of Hg complexation and their interaction with loaded metal ions.

In general, the absorbance of the peaks in the metal loaded biofilm was significantly higher than unloaded biofilm that indicated changes in the absorptivity of the functional groups due to interactions with Hg (II). The noticeable change in absorbance of hydroxyl and amine groups between 3100 and 3400 cm^{-1} and aromatic amine groups at 1200 to 1300 cm^{-1}, showed that these groups are responsible for mercury complexation and biosorption.

The interpretations above indicated that amine, hydroxyl and carboxyl groups were the main functional groups involved in the mercury biosorption process. These observations were similar to reports in previous studies on the biosorption of metals (Le Cloirec et al., 2003; Gabr et al., 2009; Joo et al., 2010; Liu et al., 2017) that reported amine, carboxyl and hydroxyl groups as the main functional groups associated with heavy metal biosorption.

3.2. Equilibrium adsorption studies

Estimation of the equilibrium adsorption of Hg(II) by living biofilm was carried out using different Hg (II) concentrations, applied to harvested geotextiles at pH 5.5, 25 °C with a contact time of 120 min. The adsorption data are shown in Fig. 2(a, b, c). Adsorption isotherms (q_e vs. C_e) are shown in Fig. 3.

3.2.1. Effect of initial concentration of Hg (II) on biosorption

Fig. 2 demonstrates the effect of initial concentration of Hg (II) on the removal efficiency and biosorption capacity using geotextiles incubated for various times (day 1, 7, 14, 21, 28). The removal percentage of different Hg(II) concentration was most altered at day 1 incubation time with a decrease from 81% to 56% for 1 mg L^{-1} and 20 mg L^{-1}, respectively. This trend was observed for all incubation times as at day 7, 14, 21 and 28 the removal efficiencies were reduced by 18%, 21%, 21% and 20%, respectively. This indicated that geotextile circles harvested after 7 days of incubation time were less altered by initial Hg(II) ion concentrations. According to Fig. 1, Hg(II) ion removal efficiencies decreased with increasing initial concentrations. The highest efficiencies were observed at 1 mg L^{-1} with 81% to 85% removal with the maximum occurring at 28 days incubation time for geotextile circles. The least removal efficiencies were observed at 20 mg L^{-1} Hg(II) concentration, ranging between 56% and 67%. This observation suggests that at higher Hg(II) concentrations the number of sorption sites were decreased. According to Fig. 2, the removal efficiencies decrease faster between 1 mg L^{-1} to 5 mg L^{-1} in comparison to 10 mg L^{-1} to 20 mg L^{-1}, that indicates the critical reduction of sorption sites in lower concentrations. This is due to the fact that at lower initial

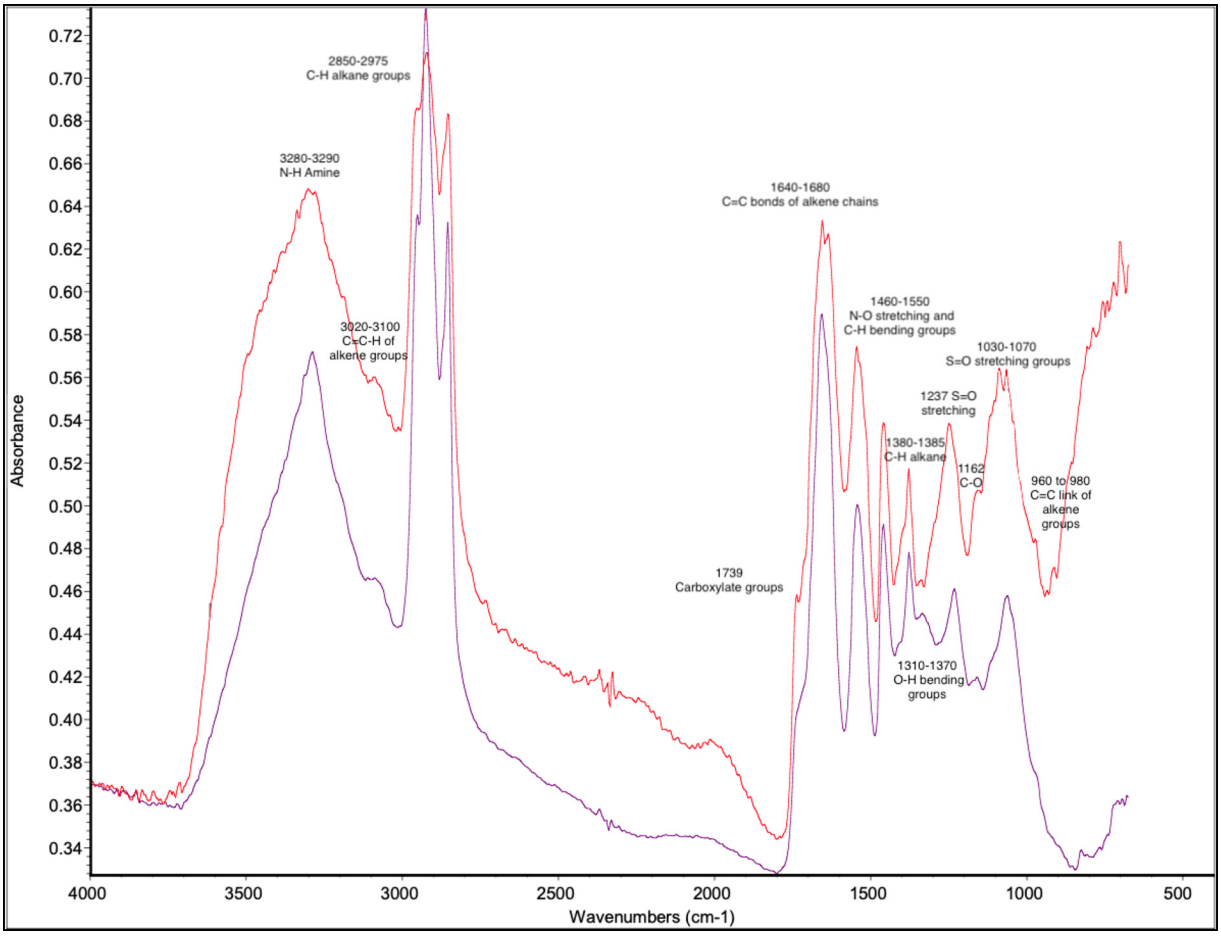

Fig. 1. FTIR spectrum of unloaded (purple) and Hg(II) loaded (red) biofilm.

concentrations the ratio of metal ions to the accessible adsorption sites of the biofilm is lower than higher concentrations that result in a higher removal efficiency. However, at higher concentrations (e.g. 10 to 20 mg L^{-1}) residual Hg(II) ions that did not occupy active biosorption sites remained in the metal solution (Radnia et al., 2012).

The Hg(II) ion equilibrium biosorption capacity increased from 7 mg g^{-1} to 101 mg g^{-1} by increasing the initial concentrations from 1 mg L^{-1} to 20 mg L^{-1} at day 1 of incubation time. At higher concentrations of Hg(II) ions, the active adsorption sites on the biofilm were covered by more Hg(II) ions, that resulted in an increased equilibrium biosorption capacity for living biofilm as the initial concentration of metal ions in aqueous solution increased (Ghorbani et al., 2008). The same pattern was observed for day 7, 14, 21 and 28 incubation times. The maximum increase in biosorption capacity was observed at day 1 with an increase of 94 mg g^{-1}. However, this increase pattern was lower with 7, 14, 21 and 28 days incubations times biofilms, showing an increase of 23 mg g^{-1}, 16 mg g^{-1}, 9 mg g^{-1} and 12 mg g^{-1}, respectively.

According to the results, the maximum biosorption capacity was observed at day 1 of incubation time, that the biofilm had the lowest mass. This observation indicated that a presumed monolayer of attached microbes at day 1, delivered the highest biosorption capacity of 101.31 mg g^{-1} for 20 mg L^{-1} initial concentration of Hg(II) ions. However, the biosorption capacity decreased as the biofilm started to develop and more layers of microbes were recruited and attached to the biofilm. According to Figs. 2 and 3, the biosorption efficiency of day 1 was as high as more developed biofilms of day 7, 14, 21 and 28, however, less developed biofilms showed higher biosorption capacities. This observation indicated that the monolayer attached biofilm was responsible for the biosorption. However, the deeper layers in more developed biofilms were less available for Hg(II) ions and as a result, were less active in the biosorption process.

3.2.2. Effect of biofilm incubation time on biosorption of Hg (II)

The effect of incubation time on Hg(II) biosorption capacities and efficiencies by the living biofilm is shown in Fig. 2. According to this figure, by increasing the initial concentration from 1 mg L^{-1} to 20 mg L^{-1} for geotextile circles incubated for 1 day, the Hg(II) uptake increased from 7 mg g^{-1} to 101 mg g^{-1}, respectively. The increase of biosorption capacity at higher concentrations was observed for all stages of biofilm development (day 1, day 7, day 14, day 21 and day 28), that was due to the higher concentration gradient acting as a force towards a facilitation of the biosorption process (Balakrishnan et al., 2017).

It was also clear that the maximum biosorption capacity occurred on the first day of biofilm development. However, the uptake capacity of the biofilm decreased as the biofilm develops further. This was due to the increase of mass and addition of new microbial layers, making the innermost layers less active in the biosorption process. The biosorption capacity increased at day 28 in comparison to day 21 that could be due to the occurrence of a dispersion stage of biofilm development and a detachment of some parts of biofilm. This led to a decrease in biofilm mass and as a result a higher biosorption capacity.

3.2.3. Control biosorption experiment

In order to evaluate the adsorption capacity of the nonwoven polypropylene-polyethylene geotextile and confirm the accuracy of

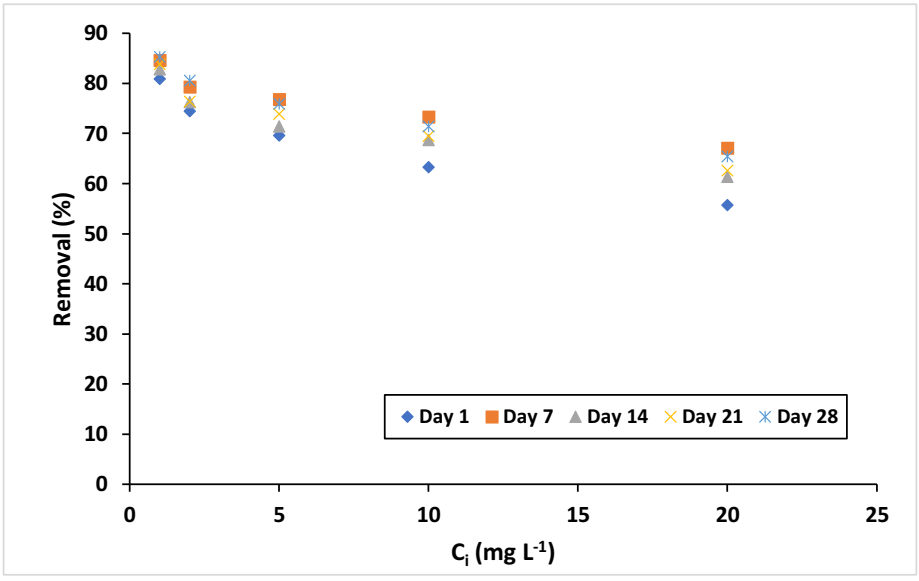

a)

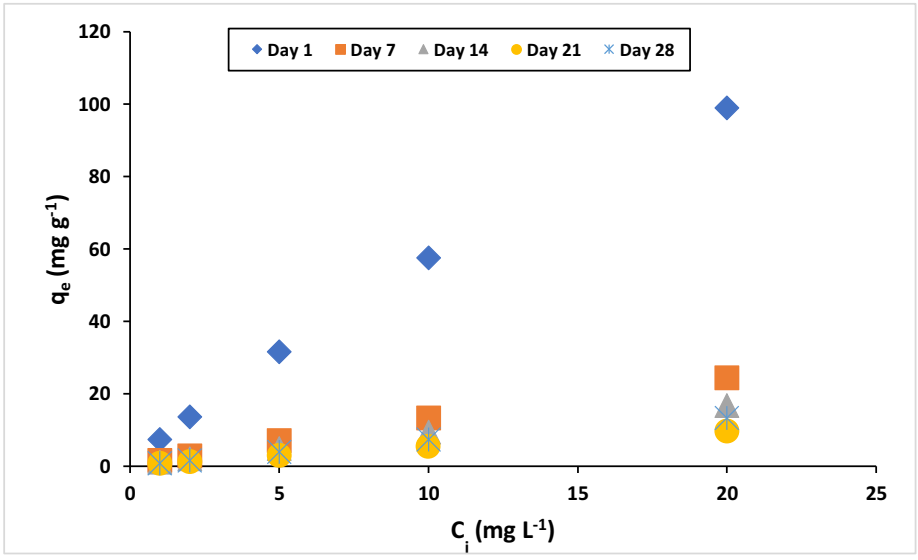

b)

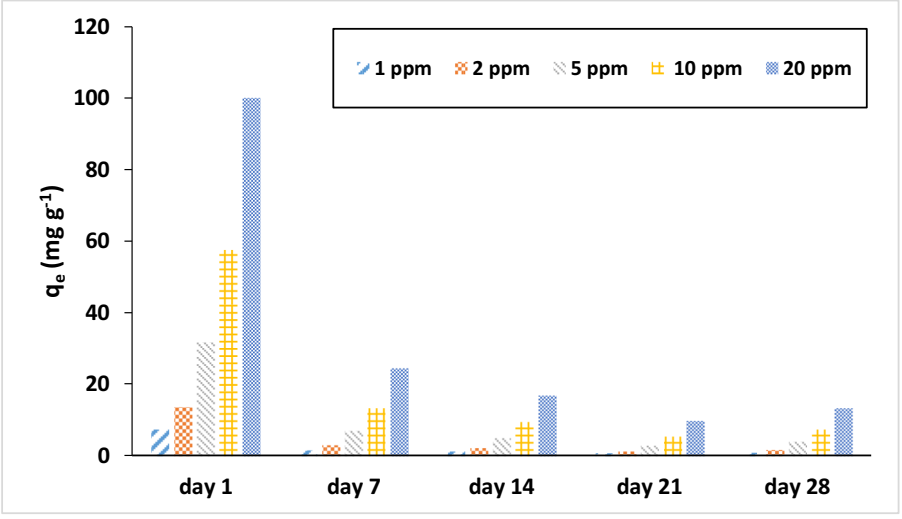

c)

Fig. 2. The effect of initial Hg(II) concentration on the removal efficiency and biosorption capacity of living biofilm at pH 5.5, 25 °C and different incubation times of living biofilm.

biosorption capacity of the living biofilm, a comprehensive set of control experiments were carried out. A sets of geotextile circles were soaked in autoclaved deionised water for a period of 28 days as well as a second set of geotextile circles soaking in a synthetic medium with same concentration of oil that was used in the bioreactor, but with no bacterial inoculum to avoid the biofilm growth. These control experiments were carried out to assess the possible effect of water and oil on adsorption capacities of the geotextile circles without biofilm growth. Geotextile circles were harvested after 28 days, prior to addition of 10 mL of 1, 10 and 20 mg L^{-1} Hg(II) solution at pH 2, 4 and 6 and 25 °C for a contact time of 120 min. Samples were taken for each Hg(II) concentration and pH prior to ICP-OES analysis.

The adsorption efficiencies of all sets of control experiments conditions were below the detection limits of the ICP-OES instrumentation. This observation indicated that soaking in deionised water and oil did not alter the adsorption behaviour of the polypropylene-polyethylene geotextile and adsorption remained negligible (below the detection limit). Control experiments showed that the geotextile filter had a negligible contribution in relation to the detected Hg (II) removal capacities of the living biofilm.

3.2.4. Modelling of equilibrium adsorption data

The equilibrium adsorption data were modelled by plotting q_e vs. C_e (see Fig. 3). The data were then fitted by applying the linearized forms of Langmuir and Freundlich isotherm equations (see Section 2.4) for the adsorption of Hg(II) onto the living biofilm incubated for varying days. The linear correlation coefficient (r^2) of Langmuir and Freundlich isotherms for biofilms with different incubation times are presented in Table 1 alongside isotherm constants. The high r^2 value in the Langmuir model suggests that the adsorption of Hg(II) primarily has occurred via a monolayer reaction, that supports the results discussed in the effect of incubation time section, and also the observed maximum biosorption capacity of geotextile filters when harvested on day 1. The Q_{max} has decreased constantly from day 1 to day 21. However, an increase of Q_{max} value at day 28 is thought to be due to the detachment phase of the biofilm growth, leading to a lower mass and as a result, a higher adsorption capacity compared with day 21.

As presented in Table 1, the r^2 value in the Freundlich model was higher than 0.995 for all stages of biofilm development, that indicated the adsorption data fitted this model. This is due to the complex and heterogeneous nature of the biofilm and the fact that Freundlich model is the best for this type of adsorbent. The K_F value decreased from day 1 to day 21, however, an increase in the K_F value in day 28 was a result of decreased biofilm mass as discussed earlier. As shown in Fig. 3, all biofilm stages from day 1 to day 28 had an L shape isotherm. The L-shaped isotherm was indicating a decreasing slope as initial concentration increased that suggested the vacant active biosorption sites on the living biofilms had decreased as the adsorption monolayer sites were covered by the Hg(II) ions. This biosorption behaviour could be described by the excessive affinity of the biofilm for the Hg(II) ions at low concentrations, that decreased as initial concentrations increased.

3.2.5. Free energy of adsorption (E)

In order to calculate the mean free energy of Hg(II) biosorption by the living biofilm, the Dubinin and Radushkevich (1947) model was applied to the experimental data. The linearized equation of D-R model is as follows:

$$\ln q_e = \ln q_m - B[R.T.\ \ln(1 + 1/C_e)]^2$$

where B is a constant related to the mean free energy of adsorption ($mol^2\ J^{-2}$); R is the gas constant (8.314 J $mol^{-1}\ K^{-1}$) and T is the temperature (K).

The free energy of adsorption E (J mol^{-1}) is calculated using the following equation (Hasany and Chaudhary, 1996):

$$E = (-2B)^{-1/2}$$

E is defined as the change in free energy when one mole of adsorbate in solution is transferred from infinity to the adsorbent surface. The E (kJ mol^{-1}) parameter is normally used to interpret the dominated biosorption process. In other words, it indicates whether the biosorption process is a chemical ion-exchange or physical adsorption. If $8 < E < 16$ kJ mol^{-1}, the adsorption is classified as a chemical or ion-exchange process; whereas if $E < 8$ kJ mol^{-1}, the biosorption is considered as a physical process. According to Table 1, it is clear that the calculated E values of different stages of biofilm growth were less than 8 kJ mol^{-1}, that indicated the biosorption of Hg(II) ions, by all stages of biofilm growth, was a physical adsorption process.

3.2.6. Effect of pH on living biofilm biosorption

Hg(II) ion uptake by biofilm depends on pH, as the speciation of Hg ions is a function of the acidity of the metal solution. Moreover, the pH of the solution affects the protonation and deprotonation of the functional groups available on the living biofilm and as a result can change the removal efficiencies (Romera et al., 2007). The pH of the Hg(II) solution affects the competition of metal and hydrogen ions to bind with the biosorbent surface (Gupta et al., 2010). Fig. SI 1 shows the species distribution of Hg(II) ions at different pH values. The effect of pH on 10 mg L^{-1} Hg (II) biosorption by living biofilm on harvested geotextiles

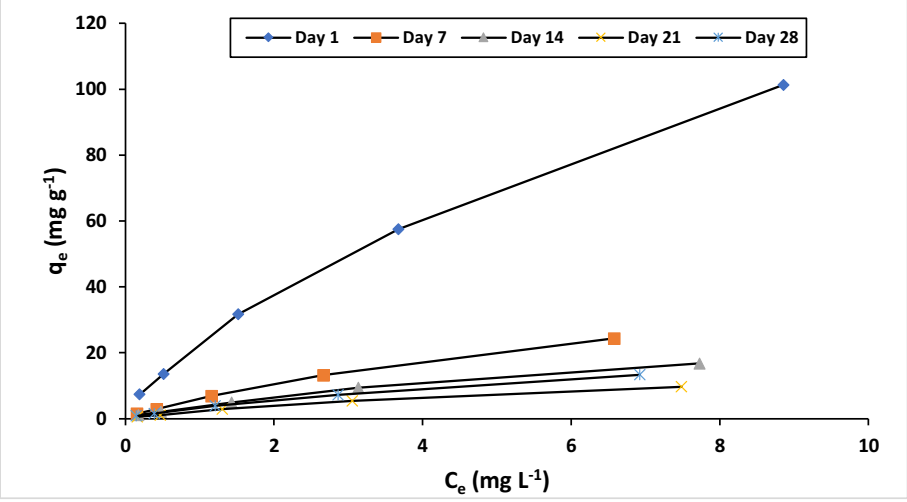

Fig. 3. Modelling of equilibrium biosorption data (q_e vs. C_e) for different incubation times of biofilms at pH 5.5, 25 °C.

Table 1
Adsorption constants of Langmuir, Freundlich and D-R isotherms.

	Langmuir Model			Freundlich Model			D-R Model	Isotherm shape
	Q_{max} (mg g^{-1})	K_L (L mg^{-1})	r^2	K_F	N	r^2	E (kJ mol^{-1})	
Day 1	154.6	0.19	0.9328	22.4	1.4	0.9987	2.24	L-1
Day 7	43.5	0.18	0.9177	6.1	1.3	0.9976	2.36	L-1
Day 14	28.2	018	0.9027	3.9	1.4	0.9973	2.24	L-1
Day 21	16.2	0.18	0.9050	2.3	1.4	0.9956	2.36	L-1
Day 28	21.4	0.21	0.9095	3.4	1.4	0.9994	2.36	L-1

at 25 °C and pH 2.0, 3.0, 4.0, 5.0, 6.0 and 7.0, was carried out in this research. The Hg(II) removal efficiency (%) and adsorption equilibrium (q_e) of 7 days incubated geotextile circles are presented in Table SI 2.

According to Table SI2 the maximum biosorption efficiency was achieved at pH 6, whereas, minimum capacities were observed at pH 2 with percentages of 73% and 66%, respectively. The observed increase of biosorption as the pH increased, was due to the fact that high concentrations and mobility of H^+ ions occupy the active sites on biofilm surface at low pH values and reduce the Hg(II) ions biosorption. The phenomena decreases with the increase of pH value, as lower concentrations of H^+ are available in the solution, and as a result more Hg (II) ions are involved in the biosorption process (Feng et al., 2011).

As discussed earlier in the FTIR section, amine, carboxyl and hydroxyl groups were the main functional groups available on this biofilm and associated with the Hg(II) biosorption process. The increase of pH leads to deprotonation of these functional groups. This deprotonation and negatively charged moieties bond with the precipitated $Hg(OH)_2$ at pH 5–6, by H-bonding or by complexation with the vacant d-orbitals of Hg (II). As was indicated in the FTIR section, it was suggested that amine, hydroxyl and carboxyl groups were involved in the mercury biosorption process. This fact describes the higher biosorption efficiencies observed at higher pH in this study. Furthermore, at lower pH, the surface of the biofilm is positively charged and as a result, pushes the positively charged Hg (II) ions away, causing a lower biosorption efficiency (Farooq et al., 2010).

3.3. Effect of temperature on biosorption (thermodynamic studies)

The effect of temperature of the metal solution on biosorption of Hg (II) ions onto living biofilm was investigated at 25 °C, 35 °C, 45 °C and 55 °C. 10 mL of Hg(II) solution at pH 5.5 with concentrations of 0.2 mg L^{-1}, 1 mg L^{-1}, 2 mg L^{-1}, 5 mg L^{-1}, 10 mg L^{-1} and 20 mg L^{-1} were applied to 7 day incubated geotextile circles for 120 min contact time. Fig. 4 illustrates the biosorption equilibrium (q_e) versus equilibrium concentration (Ce) of the living biofilm at different temperatures. This figure shows the exothermic nature of Hg(II) biosorption onto the living biofilm. The decrease in biosorption capacity and efficiency at higher temperatures was due to the tendency of Hg(II) ions to escape from the biofilm surface into the solution. This decrease of biosorption efficiency may also be attributed to destruction of adsorption active sites on the living biofilm and as a result less available biosorption capacity (Meena et al., 2005).

Thermodynamic behaviour of Hg(II) biosorption by living biofilm was carried out by calculation of the thermodynamic parameters including free energy charge (ΔG, classic Vant Hoff equation), entropy (ΔS) and enthalpy (ΔH) using the following equations (Gibbs free energy change):

$$\Delta G = -RT\ln K$$

$$K = Q_{max} K_L$$

$$\Delta G = \Delta H - T \cdot \Delta S$$

where R (8.314 J mol^{-1} K^{-1}) is the universal gas constant and T is the sorption temperature in Kelvin. Values of ΔH and ΔS were calculated by plotting the ΔG versus T and estimating the graph intercept and slope. Thermodynamic parameters (ΔG, ΔS and ΔH) of living biofilm biosorption of Hg(II) are presented in Table 2. The ΔG parameter indicates the spontaneity of the biosorption. Values of ΔG in the range of 0 to −20 $kJmol^{-1}$ are a sign of physisorption, whereas, a ΔG value between −80 to −400 kJ mol^{-1} is assigned to an adsorption with chemisorption nature. Moreover, the ΔH value specifies whether the enthalpy of the biosorption is exothermic or endothermic. Finally, the ΔS value reveals the alteration of randomness and disorder of the biosorption.

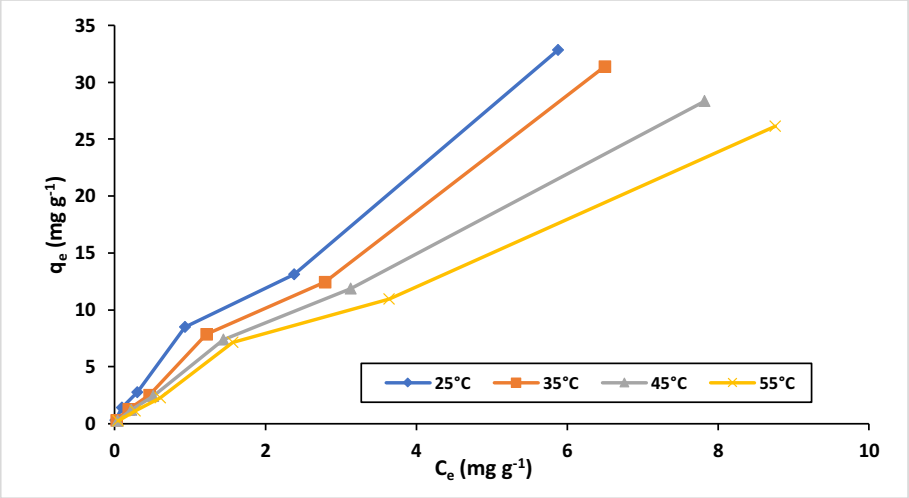

Fig. 4. Biosorption equilibrium (qe) versus equilibrium concentration (Ce) for 7 days incubated biofilms at pH 5.5, different temperatures and 120 min contact time.

Table 2
Thermodynamic parameters for biosorption of Hg(II) by living biofilm at pH 5.5.

Temp (°K)	ln K	ΔG (kJ mol^{-1})	ΔH (kJ mol^{-1})	ΔS (J K^{-1}mol^{-1})
298	2.47	−6.1	−26.2	−68
308	1.97	−5.0		
318	1.72	−4.5		
328	1.46	−4.0		

The ΔG values were calculated using the equation above and found to be −6.1, −5.0, −4.5 and −4.0 kJmol^{-1} for 25 °C, 35 °C, 44 °C and 55 °C, respectively. The negative values of ΔG in the range of 0 to −20 kJmol^{-1} indicated the physisorption nature of Hg(II) biosorption process by the living biofilm. Moreover, the negative ΔG value indicated that the living biofilm biosorption of Hg(II) was thermodynamically feasible and had a spontaneous nature. As is illustrated in Table 2, the ΔG value has increased with the increase of temperature, that indicates the adsorption process became less spontaneous at higher temperatures and thus the process became less favourable. The **Δ**H value of the biosorption process was calculated using the equations mentioned earlier and found to be −26.2 kJmol^{-1}. The negative value of **Δ**H specified the exothermic nature of the Hg(II) biosorption by the living biomass at 25 °C to 55 °C. On the other hand, the calculated value of ΔS was −68 J K^{-1} mol^{-1}, that showed the decrease in randomness during the biosorption process at the living biofilm and Hg(II) solution boundary.

3.4. Kinetics of the biosorption of Hg(II)

Kinetic studies of the biosorption process were carried out in order to better understand the mechanism for living biofilm biosorption of Hg(II) and find out the possible rate-controlling phases that involve mass transport and chemical processes. The investigation of biosorption rates provides valuable information for designing batch biosorption systems with optimum conditions (Tuzen and Sari, 2010). The kinetic biosorption data are shown in Fig. 5.a. The biosorption kinetics mechanism was investigated using pseudo-first-order and pseudo-second-order kinetic models to evaluate the kinetic experimental data. The pseudo-first-order kinetic equation (Lagergren, 1898) assumes that metal ions bind to just one biosorption site on the biosorbent (Ghaedi et al., 2013) and this is presented in the linear form as follows:

$$(qe - qt) = \ln qe - K_1 t$$

where K_1 is the pseudo-first-order rate constant (min^{-1}), q_e and q_t (mg g^{-1}) are the amount of metal ions adsorbed on the adsorbent per unit mass at equilibrium and at any time t (min), respectively. The value

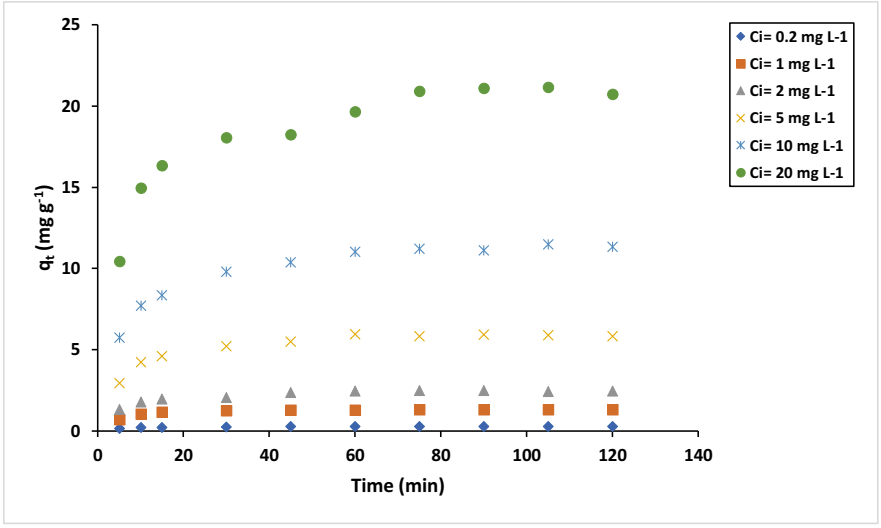

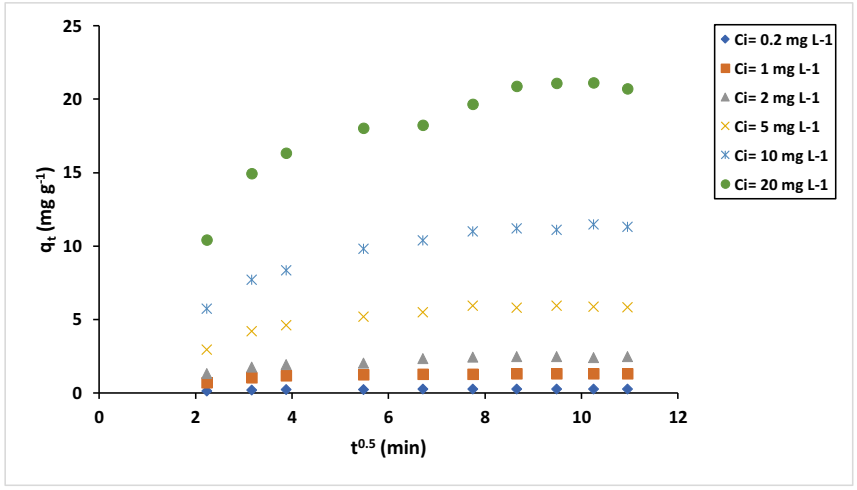

Fig. 5. a) Kinetic adsorption data. b) Intra-particle diffusion model (biosorption of Hg(II) by 7 days incubated living biofilm at pH 5.5, 25 °C).

of K_1 and q_e were calculated by plotting the graph using log (q_e - q_t) versus (t) and estimating the slope and intercept of the diagram which are presented in Table 3.

The pseudo-second-order kinetics model reported by Ho and McKay (1998) assumes that the biosorption process rate is likely to be limited by chemical interactions binding the metal ions to the biosorbent surface, using bonds as strong as covalent (Gupta and Bhattacharyya, 2011). The pseudo-second-order kinetic model equation is expressed in the linear form as follows:

$$\frac{t}{q_t} = \frac{1}{K_2 q_e^2} + \left(\frac{1}{q_e}\right)t$$

where K_2 (g mg^{-1} min^{-1}) is the second-order rate constant of adsorption. The values of K_2 and q_e are estimated by plotting t/$q_t$versus t and calculation of the slope and intercept of the graph (which are shown in Table 3) along with the corresponding regression correlation coefficients (r^2). According to Table 3 the r^2 value was higher in pseudo-second order model than pseudo-first order model and also q_e values calculated using the model were in a good match with the q_e values obtained from the experimental data. This observation reveals that the biosorption of Hg (II) by the living biofilm followed the pseudo second order kinetic model which can be used to calculate the equilibrium biosorption capacities, biosorption rate constants and Hg(II) ions removal efficiencies.

3.4.1. Intra-particle diffusion

Previous studies have shown the importance of using kinetic data in mechanism investigation of adsorption process (El-Sheikh et al., 2012). The biosorption processes are normally controlled by following three stages (Boparai et al., 2011):

1) Film or surface diffusion which is defined as mass transfer of metal ions from the solution to the surface of the sorbent.
2) Pore or intraparticle diffusion where metal ions penetrate the inner layers of the biosorbent.
3) Biosorption on interior parts of the biosorbent.

The slowest stage of these three is considered as the rate-limiting phase.

The Weber and Morris intra-particle diffusion model assumes that three previous mentioned diffusion stages occur until the surface of sorbent is saturated. The domination of intraparticle diffusion can be confirmed by evaluating the Weber and Morris (1963) equation which is expressed as follows:

$$q_t = k_{id}\, t^{0.5} + C$$

where k_{id} is the rate constant of intra-particle diffusion (mg g$^{-1/2}$ min$^{-1/2}$) and C is a constant that is related to the thickness of the boundary layer at the surface diffusion stage. Fig. 5.b is provided by plotting q_t versus $t^{0.5}$ to evaluate the existence of intraparticle diffusion of Hg(II) ions onto living biofilm at 25 °C and pH 5.5.

The shape of the graphs of q_t versus $t^{0.5}$ provides valuable information about the adsorption mechanism. Depending on whether plots have one or more than one line and also pass through the origin or not, rate limiting steps can be interpreted. The value of intercept in plotted graphs reveals the effect of the boundary layer. According to Fig. 5.b, three linear sections were present which was a sign that there were three stages involved in Hg(II) ions biosorption by the living biofilm. The sharp beginning of the graph ($t^{0.5} = 0$ to 3) revealed the diffusion of the Hg(II) ions through the solution to the outer layer of biofilm surface as film or surface diffusion occurs.

The second stage which started at $t^{0.5} = 3$ to 7, indicated the gradual biosorption process in which intraparticle diffusion was taking place and controlled the rate. The third stage ($t^{0.5} = 7$) was where the intraparticle diffusion gradually stopped due to the lower Hg(II) ion concentration in the solution. Therefore, the Hg(II) biosorption by the living biomass was a three staged process, dominated by surface biosorption and intraparticle diffusion. The intraparticle step seemed slower between $t^{0.5} = 3$ to 7 and therefore could be considered as the rate limiting stage.

3.5. Comparison with other metal attenuation studies

As a model environmental toxic metal, mercury serves as a guide for how biologically activated geosynthetics may beneficially interact with variable trace concentrations of metals from human societies. Work by Nnadi et al. (2014) and Mbanaso et al. (2020) showed that synthetic stormwater, including metal residues was treated by PPS including a geotextile, to an extent where it was shown to present a much lower environmental threat if discharged as effluent, compared with untreated runoff conveyed by traditional drainage systems. Stormwater management device options that can be deployed due to there being a large amount of available space, such as constructed wetlands, are known to be effective at runoff remediation (Usharani and Vasudevan, 2013) and to be driven by active and adaptable microbial communities in the decontamination of wastewater (Sánchez, 2017). The use of grey, engineered SuDS devices to develop adsorbent media for soluble metals, in particular on an established geosynthetic material, is new and significant advance on the concept of ecosystem services or ecosystem function for SuDS.

Other work to determine the fate of metals in paving has shown that PPS can treat zinc and copper in stormwater, reducing these metals significantly in discharge (Ostrom and Davis, 2019). It has also been shown that novel paving materials, in this case lime and sand bricks (Zhang et al., 2019), can reduce the concentration of soluble copper, and that this process was capable of reaching a maximum adsorption capacity of 7 mg g^{-1}. However, this research results showed that a living biofilm has a biosorption capacity of 9–101 mg g^{-1} for a 20 mg L^{-1} mercury solution depending on development stage of the biofilm. Zhang et al. (2019) found that physical adsorption and ion exchange were important for copper removal, which contrasts with the present study showing a predominance of physisorption in the biofilm removal of mercury. In the two referenced studies above, both strategies utilised new formulations of paving and/or sub base materials in order to achieve the metal removal, which contrasts with the 1 mm^{-1} thick geotextile employed as the adsorbent in this study. Ostrom and Davies used 50 mm^{-1} of substrate depth and Zhang et al. used a depth of 200 mm^{-1}, showing a

Table 3
Comparison of pseudo-first-order and pseudo-second-order adsorption rate constants, calculated and experimental adsorption capacities.

C_i	0.2 mg L^{-1}	1.0 mg L^{-1}	2.0 mg L^{-1}	5.0 mg L^{-1}	10.0 mg L^{-1}	20.0 mg L^{-1}
$q_{e,exp}$ (mg g^{-1})	0.3	1.4	2.5	6.0	11.0	21.0
Pseudo-1st order						
r^2	0.715	0.702	0.430	0.688	0.899	0.874
$q_{e,cal}$ (mg g^{-1})	0.086	0.325	0.721	1.816	4.677	8.570
k_1 (min^{-1})	0.012	0.015	0.040	0.030	0.020	0.021
Pseudo-2nd order						
r^2	0.999	0.999	0.998	0.999	0.999	0.998
$q_{e,cal}$ (mg g^{-1})	0.3	1.4	2.6	6.2	12.0	22
k_2(g mg^{-1}min^{-1})	0.94	0.240	0.080	0.034	0.017	0.008

significantly greater commitment of materials per unit area of pavement to achieve metal adsorption, than that found with a biologically active geotextile. What differentiates this study from other research into adsorption of stormwater-borne metals in pavements, is the proven contribution of the biofilm to the removal of mercury.

In previous PPS research, biofilms were shown to grow on geotextiles and degrade oils (Newman et al., 2002) or metals were shown to be attenuated by passage through PPS, many of which used a geotextile, but the removal mechanism for soluble metals in effluent was not determined (Nnadi et al., 2014; Mbanaso et al., 2020). In addition, in the above studies there was no clear separation of metals into dissolved and particulate fractions, only the total metal concentrations applied and released in effluent were reported. The present study specifically used only soluble mercury to examine worst case conditions. The potential for inexpensive, readily available, standard geotechnical materials to become biosorbents when colonised by naturally occurring, batch grown, allochthonous microbes has been demonstrated in this study. Indeed, the speed at which significant biosorption occurs (24 hour incubation in culture liquid) and the relative paucity of adsorption on clean geotextile, shows the affinity for mercury, even in a probable monolayer on the geotextile surface.

Design guidance on the inclusion of geotextiles for PPS has often specified that they are an extra barrier against the discharge of contaminated stormwater (Woods Ballard et al., 2015), and many PPS deployed in the field already use geotextiles, meaning that the benefits of biosorption from PPS covered geotextiles may be making a contribution to enhanced water quality across the world. It will be necessary to study this beneficial effect more fully to determine the lifetime of the microbial biomass, the possible release of adsorbed metal over time, the constituents of the biofilm organisms and the efficacy of biologically active geotextiles when challenged by other metals. It is planned to test more metals in soluble single doses, e.g. cadmium, copper, lead against biofilm covered geotextiles, with metals in combination and ultimately along with organics such as PAH, BTEX and plastic residues.

4. Conclusions

In this study, the equilibrium, thermodynamics, and kinetics of Hg (II) biosorption onto living biofilm grown on a nonwoven polypropylene and polyethylene geotextile, widely used in sustainable drainage systems were investigated regarding the impact of initial metal concentrations, contact time, temperature and pH of the solution. Investigation of the Hg(II) biosorption capacity and efficiency of different stages of biofilm development was carried out. The Langmuir, Freundlich and Dubnin Radushkevich models were used to better understand the mechanism of Hg(II) biosorption to the living biofilm. It was observed that the equilibrium concentrations fitted perfectly to the Freundlich model and with a lower degree to the Langmuir isotherm.

The thermodynamic studies indicated that the Hg(II) biosorption of living biofilm is thermodynamically feasible and has a spontaneous and exothermic nature. Moreover, kinetic studies of equilibrium data showed that Hg(II) biosorption onto living biofilm had a better correlation with pseudo second order kinetic model compared to pseudo first order model. Finally, FTIR results showed that amine, hydroxyl and carboxyl groups were the main functional groups involved in the process of Hg(II) biosorption by the living biofilm. Moreover, controlled adsorption experiment showed negligible Hg(II) removal capacity of the geotextile without living biofilm. It can be concluded that a living biofilm grown on a nonwoven polypropylene and polyethylene geotextile can be considered an efficient and clean method for the removal of mercury ions from stormwater within the structure of SuDS devices.

CRediT authorship contribution statement

AlirezaFathollahi: Conceptualization, Methodology, Validation, Formal analysis, Investigation, Resources, Writing - original draft, Writing - review & editing. **StephenJ. Coupe:** Conceptualization, Methodology, Validation, Investigation, Resources, Writing - original draft, Writing - review & editing, Supervision, Project administration. **AmjadH.El-Sheikh:** Methodology, Validation, Investigation. **LuisA. Sañudo-Fontaneda:** Writing - original draft, Writing - review & editing.

Declaration of competing interest

The authors declare that they have no known competing financial interests or personal relationships that could have appeared to influence the work reported in this paper.

Acknowledgment

We gratefully need to acknowledge the assistance of professor Alan Newman of Coventry University, for assistance in the preparation of this manuscript.

Funding

This project has received funding from the European Union's Horizon 2020 - Research and Innovation Framework Programme under the Marie Sklodowska-Curie grant No 765057, project name SAFERUP!

Appendix A. Supplementary data

Supplementary data to this article can be found online at https://doi.org/10.1016/j.scitotenv.2020.140411.

References

Abbar, B., Alem, A., Pantet, A., Marcotte, S., Ahfir, N.-D., Duriatti, D., 2017. Experimental investigation on removal of suspended particles from water using flax fibre geotextiles. Environ. Technol. 38, 2964–2978.

Allen, D., Arthur, S., Haynes, H., Olive, V., 2017. Multiple rainfall event pollution transport by sustainable drainage systems: the fate of fine sediment pollution. Int. J. Environ. Sci. Technol. 14, 639–652.

Ashley, R., Walker, L., D'Arcy, B., Wilson, S., Illman, S., Shaffer, P., Woods-Ballard, B., Chatfield, P., 2015. UK sustainable drainage systems: past, present and future. Proc. Inst. Civ. Eng. Civ. Eng 168, 125–130.

Balakrishnan, K., Zakaria, N.A., Foo, K.Y., 2017. Preparation of eco-friendly carbon aerogel via ambient pressure drying for the effective remediation of pharmaceutical contaminant, metformin. E-proceedings of the 37th IAHR World Congress, Kuala Lampur, Malaysia.

Blanck, H., Dahl, B., 1996. Pollution-induced community tolerance (PICT) in marine periphyton in a gradient of tri-n-butyltin (TBT) contamination. Aquat. Toxicol. 35, 59–77.

Boparai, H.K., Joseph, M., OíCarroll, D.M., 2011. Kinetics and thermodynamics of cadmium ion removal by adsorption onto nano zerovalent iron particles. J. Hazard. Mater. 186, 458–465.

Borne, K.E., Fassman-Beck, E.A., Tanner, C.C., 2014. Floating treatment wetland influences on the fate of metals in road runoff retention ponds. Water Res. 48, 430–442.

Coupe, S.J., Smith, H.G., Newman, A.P., Puehmeier, T., 2003. Biodegradation and microbial diversity within permeable pavements. Eur. J. Protistol. 39, 495–498.

Dubinin, M.M., Radushkevich, L.V., 1947. The equation of the characteristic curve of the activated charcoal. Proc. Acad. Sci. USSR Phys. Chem. Sect 55, 331–337.

El-Sheikh, A.H., Al-Jafari, M.K., Sweileh, J.A., 2012. Solid phase extraction and uptake properties of multi-walled carbon nanotubes of different dimensions towards some nitrophenols and chloro-phenols from water. Int. J. Environ. Anal. Chem. 92, 190–209.

Farooq, U., Kozinski, J., Khan, M.A., Athar, M., 2010. Biosorption of heavy metal ions using wheat based biosorbents—a review of the recent literature. Bioresour. Technol. 101, 5043–5053.

Feng, N., Guo, X., Liang, S., Zhu, Y., Liu, J., 2011. Biosorption of heavy metals from aqueous solutions by chemically modified orange peel. J. Hazard. Mater. 185, 49–54.

Freundlich, H.M.F., 1906. Over the adsorption in solution. J. Phys. Chem. 57, 385–471.

Gabr, R.M., Gad-Elrab, S.M.F., Abskharon, R.N.N., Hassan, S.H.A., Shoreit, A.A.M., 2009. Biosorption of hexavalent chromium using biofilm of E. coli supported on granulated activated carbon. World Journal of Microbiology & Biotechnology 25, 1695–1703.

Ghaedi, M., Hajati, S., Karimi, F., Barazesh, B., Ghezelbash, G., 2013. Equilibrium, kinetic and isotherm of some metal ion biosorption. J. Ind. Eng. Chem. 19, 987–992.

Ghorbani, F., Younesi, H., Ghasempouri, S.M., 2008. Application of response surface methodology for optimization of cadmium biosorption in an aqueous solution by Saccharomyces cerevisiae. Chem. Eng. J. 145, 267–275.

Gill, L.W., Ring, P., Higgins, N.M.P., Johnston, P.M., 2014. Accumulation of heavy metals in a constructed wetland treating road runoff. Ecol. Eng. 70, 133–139.

Gomez-Ullate, E., Bayon, J.R., Coupe, S., Castro-Fresno, D., 2010. Performance of pervious pavement parking bays storing rainwater in the north of Spain. Water Sci. Technol. 62, 615–621.
Green-Ruiz, C., Rodriguez-Tirado, V., Gomez-Gil, B., 2008. Cadmium and zinc removal from aqueous solutions by Bacillus jeotgali: pH, salinity and temperature effects. Bioresour. Technol. 99, 3864–3870.
Gupta, S.S., Bhattacharyya, K.G., 2011. Kinetics of adsorption of metal ions on inorganic materials: a review. Adv. Colloid Interf. Sci. 162, 39–58.
Gupta, V.K., Rastogi, A., Nayak, A., 2010. Biosorption of nickel onto treated alga (Oedogonium hatei): application of isotherm and kinetic models. J. Colloid Interface Sci. 342, 533–539.
Han, J.C., Gao, X.L., Liu, Y., Wang, H.W., Chen, Y., 2014. Distributions and transport of typical contaminants in different urban stormwater runoff under the effect of drainage systems. Desalin. Water Treat. 52, 1455–1461.
Hasany, S.M., Chaudhary, M.H., 1996. Sorption potential of Hare river sand for the removal of antimony from acidic aqueous solution. Appl. Radiat. Isot. 47, 467–471.
Ho, Y.S., McKay, G., 1998. A comparison of chemisorption kinetic models applied to pollutant removal on various sorbents. Process. Saf. Environ. Prot. 76, 332–340.
Huber, M., Welker, A., Helmreich, B., 2016. Critical review of heavy metal pollution of traffic area runoff: occurrence, influencing factors, and partitioning. Sci. Total Environ. 541, 895–919.
Joo, J.H., Hassan, S.H.A., Oh, S.E., 2010. Comparative study of biosorption of Zn2 by Pseudomonas aeruginosa and Bacillus cereus. Int. Biodeterior. Biodegradation 64, 734–741.
Lagergren, S., 1898. Zur theorie der sogenannten adsorption geloster stoffe. Kungliga Sevenska Vetenskapasakademiens 24, 1–39 Handlingar.
Langmuir, I., 1916. The constitution and fundamental properties of solids and liquids. J. Am. Chem. Soc. 38, 2221–2295.
Lawson, N.M., Mason, R.P., Laporte, J.M., 2001. The fate and transport of mercury, methyl mercury, and other trace metals in Chesapeake Bay tributaries. Water Res. 35, 501–515.
Le Cloirec, P., Andre, Y., Faur-Brasquet, C., Gerente, C., 2003. Engineered biofilms for metal ion removal. Rev. Environ. Sci. Biotechnol. 2, 177–192.
Le Faucheur, S., Campbell, P.G.C., Fortin, C., Slaveykova, V.I., 2014. Interactions between mercury and phytoplankton: speciation, bioavailability, and internal handling. Environ. Toxicol. Chem. 33, 1211–1224.
Lin, H., Zhu, X., Feng, Q., Guo, J., Sun, X., Liang, Y., 2019. Pollution, sources, and bonding mechanism of mercury in street dust of a subtropical city, southern China. Human and Ecological Risk Assessment. An International Journal 25, 393–409.
Liu, M., Dong, F., Zhang, W., Nie, X., Wei, H., Sun, S., Zhong, X., Liua, Y., Wanga, D., 2017. Contribution of surface functional groups and interface interaction to biosorption of strontium ions by Saccharomyces cerevisiae under culture conditions. RSC Adv. 7, 50880.
Lodeiro, C., Capelo, J.L., Oliveira, E., Lodeiro, J.F., 2019. New toxic emerging contaminants: beyond the toxicological effects. Environ Sci Pollut Res 26, 1–4.
Mamisahebei, S., Khaniki, G.R.J., Torabian, A., Nasseri, S., Naddafi, K., 2007. Removal of arsenic from an aqueous solution by pretreated waste tea fungal biomass. Journal of Environmental Health Science and Engineering 4, 85–92.
Mbanaso, F.U., Coupe, S.J., Charlesworth, S.M., Nnadi, E.O., 2013. Laboratory-based experiments to investigate the impact of glyphosate-containing herbicide on pollution attenuation and biodegradation in a model pervious paving system. Chemosphere 90, 737–746.
Mbanaso, F.U., Charlesworth, S.M., Coupe, S.J., Newman, A.P., Nnadi, E.O., 2020. State of a sustainable drainage system at end-of-life: assessment of potential water pollution by leached metals from recycled pervious pavement materials when used as secondary aggregate. Environ. Sci. Pollut. Res. 27, 4630–4639.
Meena, A.K., Mishra, G.K., Rai, P.K., Rajagopal, C., Nagar, P.N., 2005. Removal of heavymetal ions from aqueous solutions using carbon aerogel as an adsorbent. J.Hazard. Mater. B 122, 161–170.
Najera, I., Lin, C.C., Kohbodi, G.A., Jay, J.A., 2005. Effect of chemical speciation on toxicity of mercury to Escherichia coli biofilms and planktonic cells. Environ Sci Technol 39, 3116–3120.
Nascimento, A.M.A., Chartone-Souza, E., 2003. Operon mer: bacterial resistance to mercury and potential for bioremediation of contaminated environments. Genet. Mol. Res. 2, 92–101.
Newman, A.P., Pratt, C.J., Coupe, S.J., Cresswell, N., 2002. Oil bio-degradation in permeable pavements by microbial communities. Water Sci. Technol. 45, 51–56.
Nnadi, E.O., Coupe, S.J., Sañudo-Fontaneda, L.A., Rodriguez-Hernandez, J., 2014. An evaluation of enhanced geotextile layer in permeable pavement to improve stormwater infiltration and attenuation. Int. J. Pavement Eng 15, 925–932.
Ostrom, T.K., Davis, A.P., 2019. Evaluation of an enhanced treatment media and permeable pavement base to remove stormwater nitrogen, phosphorus, and metals under simulated rainfall. Water Res. 166, 115071.
Peres, E., Coste, M., Ribeyre, F., Ricard, M., Boudou, A., 1997. Effects of methylmercury and inorganic mercury on periphytic diatom communities in freshwater indoor microcosms. J. Appl. Phycol. 9, 215–227.
Radnia, H., Ghoreyshi, A.A., Younesi, H., 2012. Adsorption of Fe(II) ions from aqueous phase by chitosan adsorbent: equilibrium, kinetic, and thermodynamic studies. Desalin. Water Treat. 50, 348–359.
Rajeshkumar, S., Liu, Y., Zhang, X., Ravikumar, B., Bai, G., Li, X., 2018. Studies on seasonal pollution of heavy metals in water, sediment, fish and oyster from the Meiliang Bay of Taihu Lake in China. Chemosphere 191, 626–638.
Rani, M.J., Hemambika, B., Hemapriya, J., Kannan, V.R., 2010. Comparative assessment of heavy metal removal by immobilized and dead bacterial cells: a biosorption approach. African Journal of Environmental Science and Technology 4, 77–83.
Rodriguez Martin, J.A., De Arana, C., Ramos Miras, J.J., Gil, C., Boluda, R., 2015. Impact of 70 years urban growth associated with heavy metal pollution. Environ. Pollut. 196, 156–163.
Romera, E., Gonzalez, F., Ballester, A., Blazquez, M.L., Munoz, J.A., 2007. Comparative study of biosorption of heavy metals using different types of algae. Bioresour. Technol. 98, 3344–3353.
Sabater, S., Guasch, H., Ricart, M., Romani, A., Vidal, G., Kluender, C., Schmitt-Jansen, M., 2007. Monitoring the effect of chemicals on biological communities. The biofilm as an interface. Anal. Bioanal. Chem. 387, 1425–1434.
Sánchez, O., 2017. Constructed Wetlands Revisited: Microbial Diversity in the Omics Era Microbial Ecology. 73. Heidelberg, pp. 722–733.
Sañudo Fontaneda, L.A., Blanco-Fernández, E., Coupe, S.J., Carpio, J., Newman, A.P., Castro-Fresno, D., 2016. Use of Geosynthetics for Sustainable Drainage, Sustainable Surface Water Management: A Handbook for SUDS.
Sañudo-Fontaneda, L.A., Coupe, S.J., Charlesworth, S.M., Rowlands, E.G., 2018. Exploring the effects of geotextiles in the performance of highway filter drains. Geotext. Geomembr. 46, 559–565.
Scott, J.A., Karanjkar, A.M., Rowe, D.L., 1995. Biofilm covered granular activated carbon for decontamination of streams containing heavy metals and organic chemicals. Miner. Eng. 8, 221–230.
Spicer, G.E., Lynch, D.E., Newman, A.P., Coupe, S.J., 2006. The development of geotextiles incorporating slow-release phosphate beads for the maintenance of oil degrading bacteria in permeable pavements. Water Sci. Technol. 54, 273–280.
Subhashini, S., Kaliappan, S., Velan, M., 2011. Removal of heavy metal from aqueous solution using Schizosaccharomyces pombe in free and alginate immobilized cells. 2nd International Conference on Environmental Science and Technology. 6. IACSIT Press, Singapore, pp. 2107–2111.
Sweileh, J.A., Misef, K.Y., El-Sheikh, A.H., Sunjuk, M.S., 2014. Development of a new method for determination of Al in Jordanian foods and drinks: solid phase extraction and adsorption of Al3+-D-mannitol on carbon nanotubes. J. Food Compos. Anal. 33, 6–13.
Theophilus, S.C., Mbanaso, F.U., Nnadi, E.O., Onyedeke, K.T., 2018. Investigation of the effects of slow-release fertilizer and struvite in biodegradation in filter drains and potential application of treated water in irrigation of road verges. Environ. Sci. Pollut. Res. 25, 19298–19312.
Tsekova, K., Todorova, D., Ganeva, S., 2010. Removal of heavy metals from industrial wastewater by free and immobilized cells of Aspergillus niger. Int. Biodeterior. Biodegrad. 64, 447–451.
Tuzen, M., Sari, A., 2010. Biosorption of selenium from aqueous solution by green algae (Cladophora hutchinsiae) biomass: equilibrium, thermodynamic and kinetic studies. Chem. Eng. J. 158, 200–206.
Usharani, B., Vasudevan, N., 2013. Impact of heavy metal toxicity and constructed wetland system as a tool in remediation. Environmental and Occupational Health 71, 102–110.
Vadas, T.M., Smith, M., Luan, H., 2017. Leaching and retention of dissolved metals in particulate loaded pervious concrete columns. J. Environ. Manag. 190, 1–8.
Viraraghavan, T., Srinivasan, A., 2011. Chapter: Fungal biosorption and biosorbents. Microbial Biosorption of Metals, pp. 143–158.
Volesky, B., 2003. Biosorption process simulation tools. Hydrometallurgy 71, 179–190.
Weber, W.J., Morris, J.C., 1963. Kinetics of adsorption on carbon from solution. J Sanit Eng Div Am Soc Civ Eng 89, 31–60.
Woods Ballard, B., Wilson, S., Udale-Clarke, H., Illman, S., Scott, T., Ashley, R., Kellagher, R., 2015. The SuDS Manual.
Zhang, X., Guo, S., Liu, J., Zhang, Z., Song, K., 2019. A study on the removal of copper (II) from aqueous solution using lime sand bricks. Appl. Sci. 9, 670.
Zhao, Y., Zhou, S., Zhao, C., Valeo, C., 2018. The influence of geotextile type and position in a porous asphalt pavement system on Pb (II) removal from stormwater. Water 10, 1205.